Diaphragm design guidelines and an optical pressure sensor based on MEMS technique

Xiaodong Wang[a,*], Baoqing Li[a], Onofrio L. Russo[a], Harry T. Roman[b], Ken K. Chin[a], Kenneth R. Farmer[a]

[a]*Department of Physics, New Jersey Institute of Technology, Newark, NJ 07102, USA*
[b]*PSE&G Company (T-10A) 80 Park Plaza, P.O. Box 570 Newark, NJ 07102, USA*

Abstract

The design guidelines for micro diaphragm-type pressure sensors have been established by characterization of the relationships among diaphragm thickness, side length, sensitivity, and resonant frequency. According to the study, the thickness need to be thin and the side length need to be small in order to get the sensitive diaphragm with high resonant frequency. A Fabry–Perot based pressure sensor has been designed based on the guidelines, fabricated and characterized. In principle, the sensor is made according to Fabry–Perot interference, which is placed on a micro-machined rectangular silicon membrane as a pressure-sensitive element. A fiber-optic readout scheme has been used to monitor sensor membrane deflection. The experimental results show that the sensor has a very high sensitivity of 28.6 mV/Pa, resolution of 2.8 Pa, and up to 91 kHz dynamic response.
© 2005 Elsevier Ltd. All rights reserved.

1. Introduction

Over the last decade, silicon pressure sensors have undergone a significant growth and substantial research has been carried out on micromachined, diaphragm-type pressure sensors [1–5]. In most cases, these microelectromechanical devices are manufactured from rectangular or circular diaphragms. The development of high-performance diaphragm is of critical importance in the successful realization of the devices. In particular, diaphragms capable of linear deflection are needed in many pressure sensors. In order to get the high sensitivity, the diaphragm thickness should be thin to maximize the load-deflection responses. On the other hand, thin diaphragm under high pressure may result in large deflection and nonlinear effects that are not desirable. And for the purpose of dynamic measurement, resonant frequency of the diaphragm is also an important parameter. It is therefore important to characterize the relationships among diaphragm thickness, side length, sensitivity, and resonant frequency in order to establish the design guidelines for micro diaphragm-type pressure sensors.

Optical fiber-based sensors have been shown to be attractive devices which measure a wide range of physical and chemical parameters, because the sensors have a number of inherent advantages, including small size, lightweight, high sensitivity and immunity to Electromagetic interference (EMI) noise [6–12]. A Fabry–Perot based pressure sensor has been designed, fabricated and characterized. In principle, the sensor is made according to Fabry Perot interference, which is placed on a micro-machined rectangular silicon membrane as a pressure-sensitive element. A fiber-optic readout scheme has been used to monitor sensor membrane deflection.

2. Diaphragm design guideline

The load-deflection method is a well-known method for the measurement of elastic properties of thin films. In this technique, the deflection of a suspended film is measured as a function of applied pressure. The load-deflection
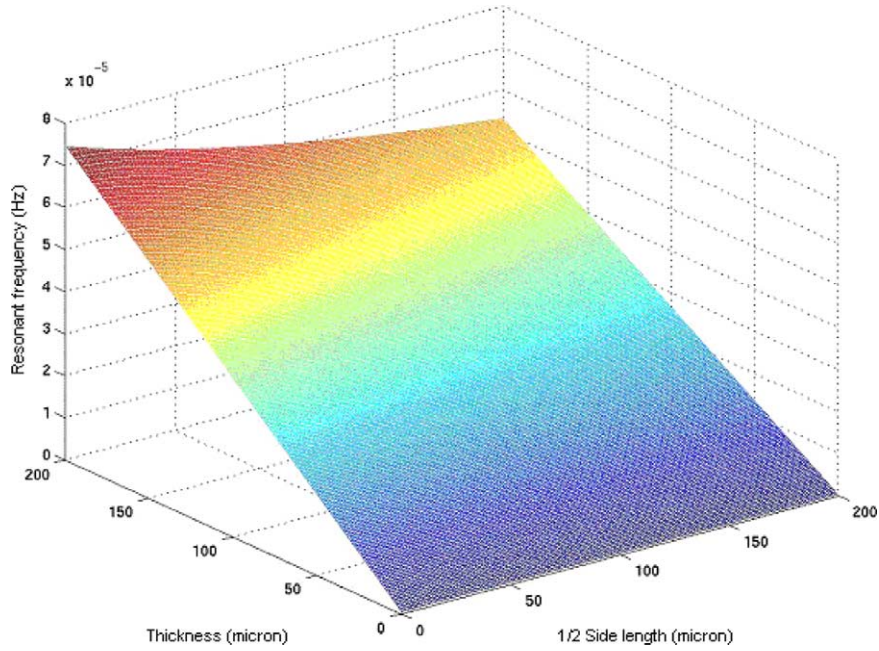
Fig. 1. The relationships among the side length, thickness, and resonant frequency at a given pressure.

relationship of a flat square diaphragm is given by [13]

$$\frac{Pa^4}{Eh^4} = \frac{4.2}{(1-v^2)}\left[\frac{y}{h}\right] + \frac{1.58}{(1-v)}\left[\frac{y}{h}\right]^3 \qquad (1)$$

Where

    P applied pressure (Pascal),
    y center deflection of diaphragm
    a half of side length,

    E young's modulus,
    h the diaphragm thickness,
    v Poisson's ratio of diaphragm material.

The deflection range is divided into two regions: a small deflection region and (deflection less than 25% of the diaphragm thickness) described by the linear term in Eq. (1), and a large deflection region described by the non-linear, cubic term in Eq. (1).
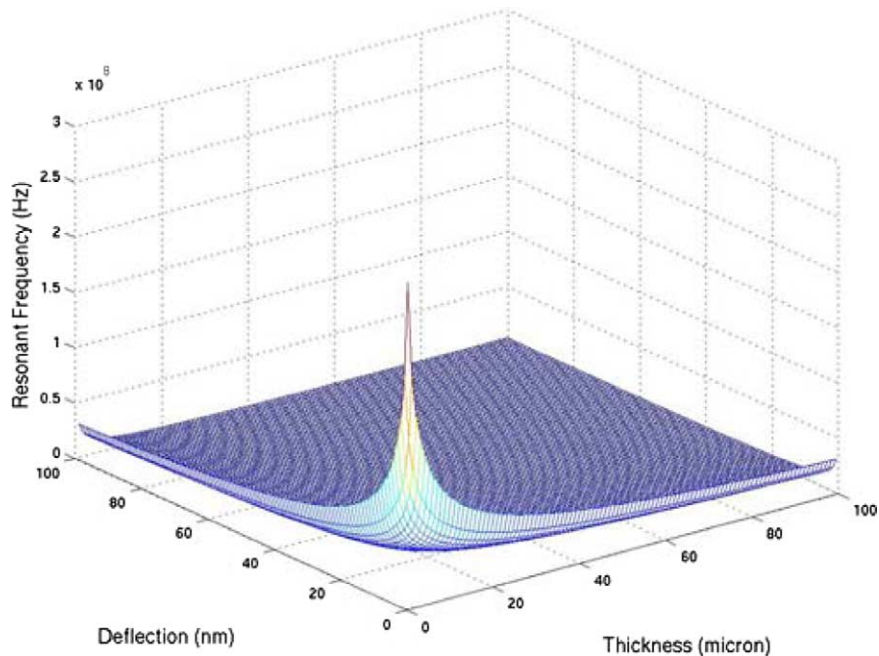

Fig. 2. The relationships among the resonant frequency, deflection and thickness of diaphragm at a given pressure.
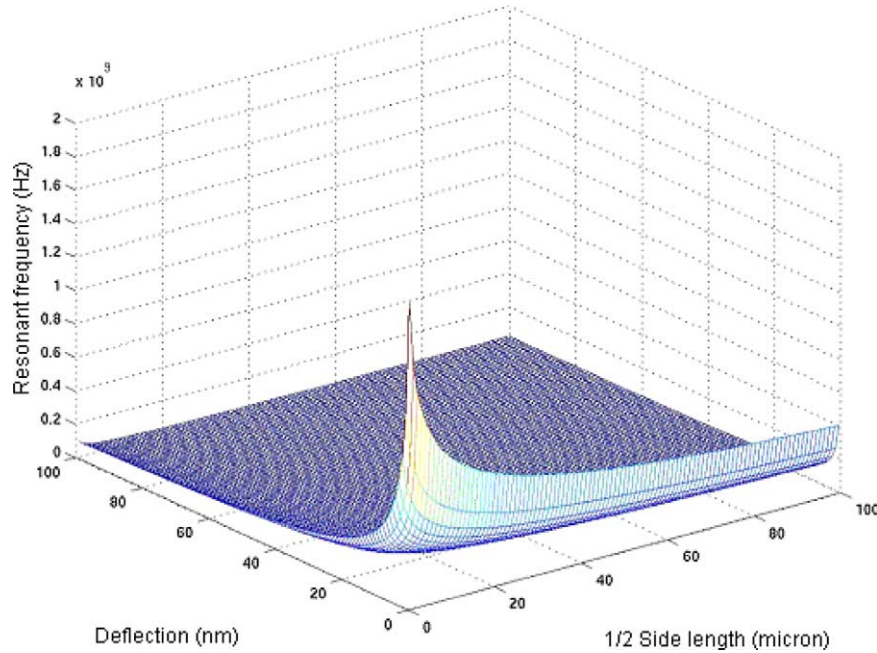
Fig. 3. The relationship among the resonant frequency, deflection and side length of diaphragm at a given pressure.

For linear Part

$$y = \frac{Pa^4(1-\nu^2)}{4.2Eh^3} \tag{2}$$

For a diaphragm clamped on its edges, from a mathematical point of view, the diaphragm can be viewed as a thin plate and the exact solution for the differential equation that describes its oscillation is given in [14]. Assuming that the deflection of the diaphragm is small compared to its thickness, the Reyleigh–Ritz method [15] can be used to find the frequency of the lowest mode of vibration. The frequency for a square plate having density ρ_d and osculating in a medium with density of ρ_m was found to be

$$f_1 = \frac{10.21}{a^2\sqrt{1+\beta}}\sqrt{\frac{gD}{\rho_d h}} \tag{3}$$

where g is acceleration of gravity, β and D are given by:

$$\beta = 0.6689\frac{\rho_m}{\rho_d}\frac{a}{h}$$

$$D = \frac{Eh^3}{12(1-\nu^2)}$$

Fig. 1 shows the relationships among half of side length, thickness, and resonant frequency. With a given side length, resonant frequency increases with thickness. With a given thickness of diaphragm, frequency decreases with side length. The figure also shows that diaphragm thickness has more effect on resonant frequency than side length.

According to Eq. (2), the half of side length can be expressed by

$$a = \left(\frac{4.2Eh^3y}{(1-\nu^2)P}\right)^{1/4}$$

By integration of expression of half of side length into Eq. (3)., resonant frequency can be expressed by

$$f_1 = \frac{4.98}{h^2}\left[\frac{(1-\nu^2)PgD}{Ey\rho_d(1+\beta)}\right]^{1/2}$$

The relationships among natural frequency, deflection and thickness of diaphragm at a given pressure are shown in Fig. 2. The figure shows that in order to get large natural frequency and large deflection, the thickness should be thin.
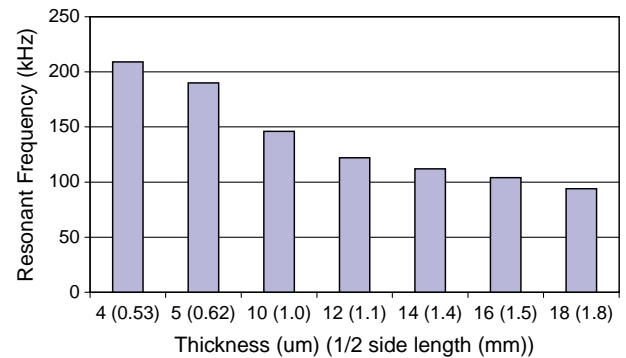

Fig. 4. Simulation results for dimensions and resonant frequency of square diaphragms with 1 nm deflection at a pressure of 1 Pa.
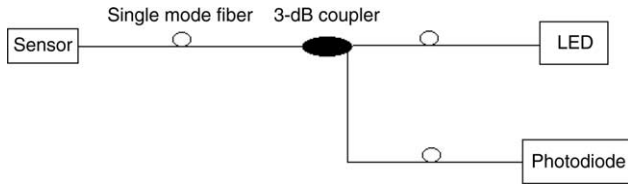
Fig. 5. Operation principle of the fiber optical sensor.

According to Eq. 2, the diaphragm deflection can be expressed by

$$h = \left[\frac{Pa^4(1-\nu^2)}{4.2Ey}\right]^{1/3}$$

Eq. 3 becomes

$$f_1 = \frac{12.97}{a^{8/3}}\left[\frac{gD}{\rho_d(1+\beta)}\right]^{1/2}\left[\frac{Ey}{P(1-\nu^2)}\right]^{1/6}$$

The relationships among natural frequency, deflection and diameter of diaphragm at a given pressure are shown in Fig. 3. The figure shows that in order to get large natural frequency and large deflection of diaphragm, the side length need to be small.

Figs. 2 and 3 shows in order to get the large deflection and large resonant frequency of the diaphragm, both the side length and thickness of the diaphragm should be small.

Fig. 4 shows simulation results for dimensions and resonant frequency of square diaphragms if the diaphragm deflection is 1 nm at the pressure of 1 Pa. According to the figure, in order to achieve larger resonant frequency at given diaphragm deflection, both the thickness and side length of diaphragm need to be smaller.

3. Sensor operation principle

The sensor system shown in Fig. 5 consists of a sensor probe, a 1310-nm LED, a 3-dB fiber optic coupler, a low noise optical receiver (photodiode) and single-mode fibers linking the sensor and the optical receiver. In the system, a laser source (1310 nm) is used as the light source, and an optical signal is converted to an electrical signal by the photodiode. The light is launched into the sensor through the coupler. The light reflected from the sensor is transmitted back through the coupler to the photodiode.

The sensor described here has just one fiber. It consists of a Fabry–Perot interferometer integrated into a single mode optical fiber. This interferometer converts the phase changes into variations of the reflected and transmitted optical power. The optical sensor is illustrated schematically in Fig. 6. The incident light is first partially reflected (R_1) at the end face of the fiber. The remainder of the light propagates across an air gap to the inner surface of the diaphragm, where it is once again partially reflected (R_2). The multiple reflections travel back along the same fiber and through the fiber coupler to the optical receiver. The received optical intensity I_r can be expressed by [16]

$$I_r = I_0 \frac{R_1 + R_2 - 2\sqrt{R_2 R_1}\cos(\phi)}{1 + R_2 R_1 - 2\sqrt{R_2 R_1}\cos(\phi)} \tag{4}$$

where I_0 is laser source power, ϕ the round trip phase shift of the light inside the air gap and given by

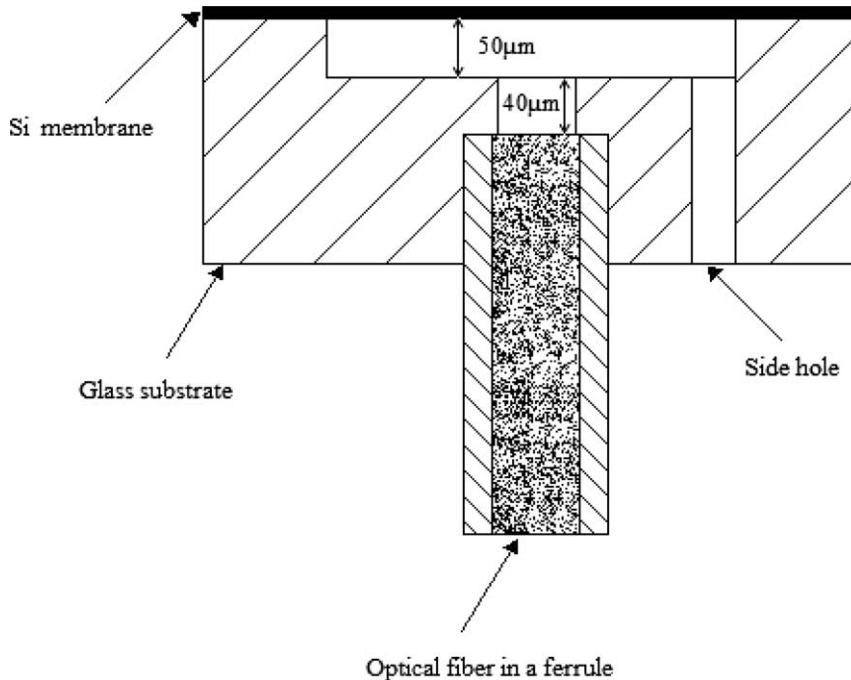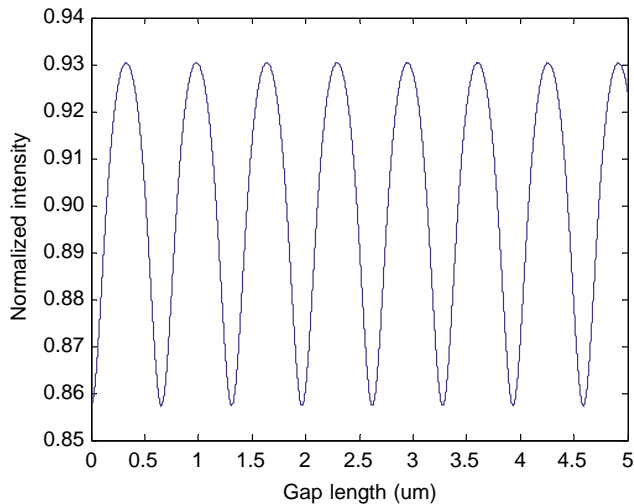$$\phi = \frac{4\pi nL}{\lambda} \tag{5}$$

Fig. 6. Sensor head design.

Fig. 7. The relationship between normalized intensity and gap length.

where L is the length of the air gap, $n = 1$ the refractive index of the air, and λ the wavelength of the light source.

The pressure causes deflection of the diaphragm and modulates the air-gap length. The sensor therefore yields outputs that correspond to the applied acoustic signals. The output signal from the sensor system should be a periodic function of changes in the gap length. Summarizing, although the circuit provides time-series data, the output is a spatially varying function of changes in the sensor gap length. It is useful to plot the detected intensity versus gap length L, as shown in Fig. 7. According to Fig. 7, a fringe period corresponds to an air-gap change of one half of the optical wavelength, which in our case is 655 nm.

If the pressure is applied to the diaphragm and causes the gap length changes by ΔL (diaphragm center deflection), the round trip optical phase change will be $\Delta\phi = 4\pi n \Delta L/\lambda$. With the assumption of uniform diaphragm thickness, small deflections, infinitely rigid clamping about the periphery of the square diaphragm, and perfectly elastic behavior, which is almost true for the silicon diaphragm and our bonding method, the linear relationship between a diaphragm center deflection and pressure difference P can be expressed as Eq. (2).

The thickness and side length of the diaphragm are selected depending upon the pressure range within which the device is required to operate. Due to high sensitivity requirement, silicon diaphragm with a thickness of 25 μm and a side length of 2 mm is selected. The expected resonant frequency is 92 kHz.

4. Fabrication of the sensor

The pressure sensor (as shown in Fig. 6), consisting of a thin silicon diaphragm and a micro-machined substrate (500 μm thick Pyrex 740 glass wafer) with a cavity and a hole for the fiber, is fabricated in a clean room in one step: anodic wafer bonding using the EV501 bonder. In order to

Fig. 8. A packaged sensor.

increase the reflectance, about 100 angstroms of gold is evaporated on the silicon diaphragm. The wafer is then diced and individual sensors are separated for packaging.

The depth of square cavity is 50 μm. A center hole in glass substrate is used to place a ferruled fiber. The cavity between the fiber end and glass surface is 105 μm wide and 40 μm deep. The width of the cavity is smaller than the fiber diameter so that the cavity serves as a stop for the fiber and sets the baseline depth of the fiber. The final chip size is about 3×3 mm. The total chip thickness is around 530 μm. An additional hole with the diameter of 400 μm drilled through the glass wafer into the cavity allows pressure measurements to be related to the surrounding pressure.

A stainless steel housing for the sensor has the sensor placed at one end as shown in Fig. 8. A 7 in. long tube is attached to a drain plug by a compression fitting. The end of the housing opposite the sensor contains a stainless steel tee fitting. One fitting of the tee is for the optical fiber and the other is to control the sensor backside pressure and environment.

5. Sensor testing

The sensor testing includes three parts: sensitivity, frequency response and resolution.

5.1. Sensitivity

The sensor sensitivity experimental setup is shown in Fig. 9. The sensor was initially immersed in the water.
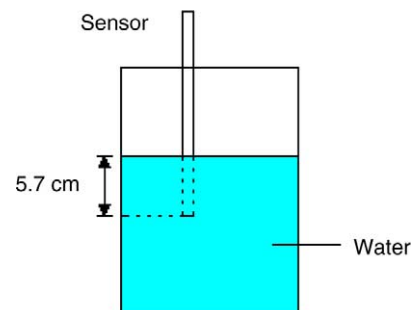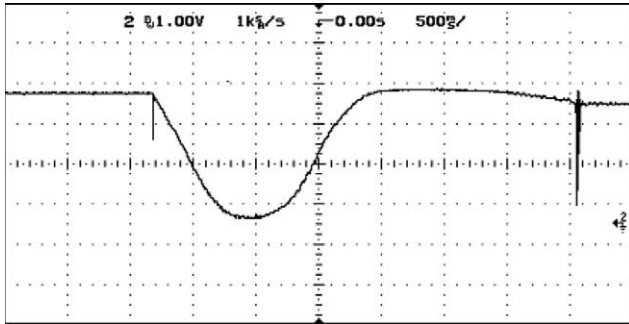

Fig. 9. Sensitivity experimental setup.

Fig. 10. Sensor one fringe output.

As the sensor was pulled out of the water, a pulse can be seen in the oscilloscope. Then according to the depth for the sensor immersed in the water, the pressure can be calculated related with the pulse. When the depth is 5.7 cm, the sensor output which is about one fringe is shown in Fig. 10. This means that the sensor had the output of a fringe period when about 558 Pa (5.7 cm water pressure) is applied to it. Since each fringe period indicates that the gap length has changed by half of the laser wavelength, 1 fringe indicates that the diaphragm deflection is 655 nm. Considering the diaphragm thickness of 25 μm and a small deflection the diaphragm deflection is linear with respect to the applied pressure if the deflection is smaller than 6.25 μm.

When the sensor is initially put close to a computer speaker which is connected to a function generator and moved away from the speaker, the output was shown in Fig. 11. The figure shows that when the sensor move away from the sound source, the number of the fringe decrease with decreased the sound pressure applied to the sensor.

5.2. Frequency response

A function generator which are connected to a computer speaker was used to produce acoustic waves. The sensor detects signals from the function generator. Then the detected signals were sent to the digital oscilloscope for demonstration. Figs. 12 and 13 shows the sensor output when the function generator produced 10 and 20 kHz signals.
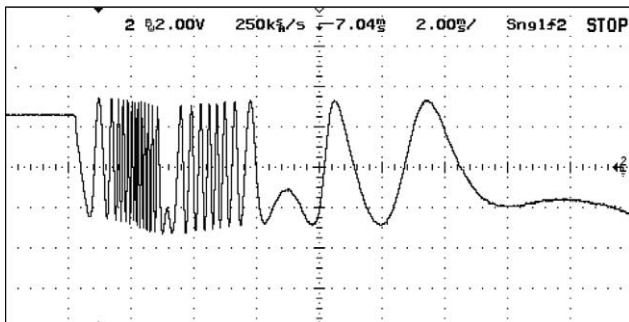

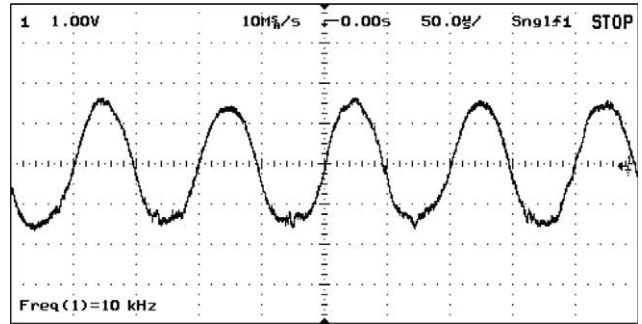Fig. 11. Sensor responses to the sound from a speaker.

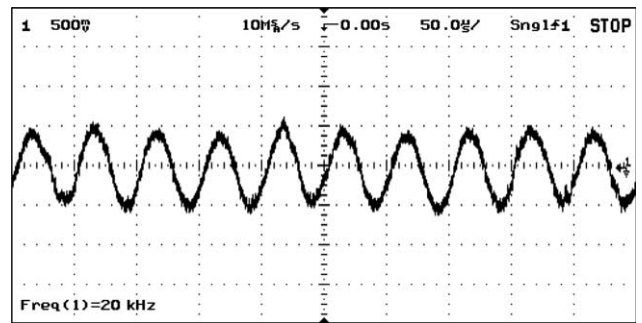Fig. 12. The sensor output of 10 kHz acoustic signal.

Fig. 13. The sensor output of 20 kHz acoustic signal.

The sensor is also used to measure the acoustic signal with a single frequency (1 kHz, 2 kHz, up to 100 kHz) generated by the function generator. The sensor output is sent to a dynamic siganl analyzer (Standford research system model SR785) for spectrum measurements. The resulting measurement scans show received power in the desired frequency, and in decibels relative to mW (dBm).

Fig. 14 shows the sensor response to acoustic signals with same amplitude and increasing frequencies, up to 100 kHz. For this measurement, the diaphragm has an expected resonant frequency of about 90 kHz. The sensor is seen to have a fairly broad resonance centered on about 90 kHz, with small structure peaks below this frequency. It shows that the sensor has a dynamic reposnse that is close to the expected value.
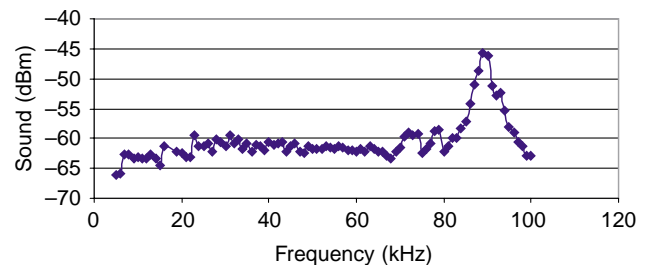

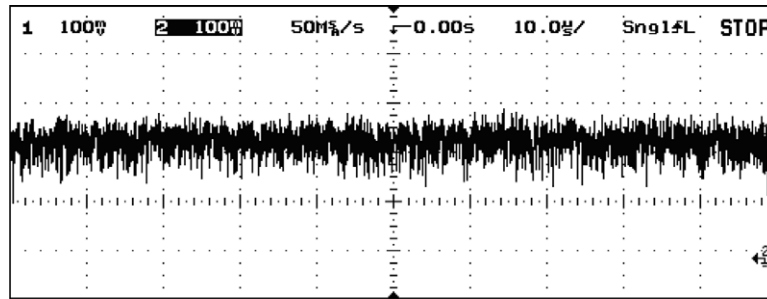Fig. 14. Frequency response of the fiber optical sensor.

Fig. 15. Noise levels of the sensor.

5.3. Resolution

The pressure measurement resolution of a sensor is limited by the signal-to-noise ratio of the sensor. According to Fig. 15, the output of the optical fiber sensor noise is around 100 mV. The output of the sensor is from −4 to 4 V corresponding to a half of a period. Since one period corresponds to about 559 Pa of applied pressure, the pressure measurement resolution of a sensor is about 2.8 Pa.

6. Conclusions

The design guidelines for micro diaphragm-type pressure sensors have been established by characterization of the relationships among diaphragm thickness, side length, sensitivity, and resonant frequency. According to the investigations, the thickness need to be thin and the side length need to be small in order to get the sensitive diaphragm with high resonant frequency. An optical fiber sensor with ultra-sensitivity is designed, fabricated, and tested. The results indicate that the sensor has a very high sensitivity (28.6 mV/Pa), the resolution of 2.8 Pa and up to 90 kHz dynamic response. A simple micromachining process compatible with MEMS has been developed for fabricating the optical fiber sensor. The use of MEMS technology is advantageous because of the potential for enormous economical manufacturing.

Acknowledgements

References

[1] W.H. Ko, Solid-state capacitive pressure transducers, Sens. Actuators 10 (1986) 303–320.

[2] H.L. Chau, K.D. Wise, Scaling limits in batch-fabricated silicon pressure sensors, IEEE Trans. Electron Devices ED-34 (1987) 850–858.

[3] K. Suzuki, S. Suwazono, T. Ishihara, Cmos integrated silicon pressure sensor, IEEE J. Solid-State Circuits SSC-22 (1987) 151–156.

[4] J.T. Kung, H.-S. Lee, An integrated air-gap-capacitor pressure sensor and digital readout with sub-100 attofarad resolution, IEEE J. Microelectromech. Syst. 1 (1992) 121–129.

[5] C.H. Mastrangelo, X. Zhang, W.C. Tang, Surface-micromachined capacitive differential pressure sensor with lithographically defined silicon diaphragm, IEEE J. Microelectromech. Syst. 5 (1996) 89–105.

[6] Y. Kim, D.P. Neikirk, Micromachined Fabry–Perot cavity pressure transducer, IEEE Photonics Technol. Lett. 7 (1995) 1471–1473.

[7] J. Han, D.P. Neikirk, Deflection behavior of Fabry–Perot pressure sensors having planar and corrugated membrane in: R. Roop, K. Chau (Eds.), SPIE's Micromachining and Microfabrication'96 Symposium: Micromachined Devices and Components II: Proceedings of SPIE 2882 (Austin, USA, 14–15 October) (1996), pp. 79–90.

[8] M.J. Gander, W.N. MacPherson, D.C. J, R. Stevens, K.S. Chana, S.J. Anderson, T.V. Jones, Embedded micromachined fiber-optic Fabry–Perot pressure sensors in.aerodynamics applications, Sens. J. IEEE 3 (2003) 102–107.

[9] R.A. Pinnock, Optical pressure and temperature sensors for aerospace applications, Sens. Rev. 18 (1998) 32–38.

[10] D. Angelidis, P. Parsons, Optical micromachined pressure sensor for aerospace applications, Opt. Eng. 31 (1992) 1638–1641.

[11] M.H. Beggans, D.I. Ivanov, S.G. Fu, T.G. Digges Jr., K.R. Farmer, Optical pressure sensor head fabrication using ultra-thin silicon wafer anodic bonding, Proc. SPIE Int. Soc. Opt. Eng. 3680 (1999) 773–782.

[12] A. Mendez, T.F. Morse, K.A. Ramsey, Micromachined Q3 Fabry-Perot interferometer with corrugated silicon membrane for fiber optic sensing applications, Proc. SPIE Int. Soc. Opt. Eng. 1793 (1993) 170–182.

[13] M.D. Giovanni, Flat and Corrugated Membrane Design Handbook, Mercel Dekker Inc, New York, 1982.

[14] P.M. Morse, K.U. Ingard, Theoretical Acoustic, McGraw-Hill, New York, 1968. pp. 209–222.

[15] C.M. Harrays, Shock and Vibration Handbook, McGraw-Hill, New York, 1966. pp. 7.38–7.45.

[16] K. Betzler, 2002, Fabry–Perot Interferometer.